

Understanding the shear modulus of dense microgel suspensions

Maxime Bergman,^{1†} Yixuan Xu,^{2†} Zhang Chi,¹,
Thomas G. Mason,^{3,4} and Frank Scheffold,^{1*}

¹Department of Physics and NCCR Bio-inspired Materials
, University of Fribourg, 1700 Fribourg, Switzerland

²Department of Materials Science and Engineering, University of California - Los Angeles, USA

³Department of Physics and Astronomy, University of California - Los Angeles, USA

⁴Department of Chemistry and Biochemistry, University of California - Los Angeles, USA

† These authors contributed equally to this work

* Correspondence to frank.scheffold@unifr.ch

Abstract

Polymer microgels exhibit intriguing macroscopic flow properties arising from their unique microscopic structure. Microgel colloids comprise a crosslinked polymer network with a radially decaying density profile, resulting in a dense core surrounded by a fuzzy corona. Notably, microgels synthesized from poly(N-isopropyl acrylamide) (PNIPAM) are thermoresponsive, capable of adjusting their size and density profile based on temperature, above the lower critical solution temperature ($T_{LCST} \sim 33$ °C), the microgel's polymer network collapses, expelling water through a reversible process. Conversely, below 33 °C, the microgel's network swells, becoming highly compressible and allowing overpacking to effective volume fractions exceeding one. Under conditions of dense packing, microgels undergo deformation in distinct stages: corona compression and faceting, interpenetration, and finally, isotropic compression. Each stage exhibits a characteristic signature in the dense microgel suspensions' yield stress and elastic modulus. Here, we introduce a model for the linear elastic shear modulus by minimizing a quasi-equilibrium free energy, encompassing all relevant energetic contributions. We validate our model by comparing its predictions to experimental results from oscillatory shear rheology tests on microgel suspensions at different densities and temperatures. Our findings demonstrate that combining macroscopic rheological measurements with the model allows for temperature-dependent characterization of polymer interaction parameters.

In the last few decades, the polymer-colloid duality of microgels has captured the interest of scientists from various fields (1,2). Microgels are cross-linked polymer networks that are typically suspended in water and exhibit properties that lie between those of macroscopic polymer gels and colloids. When the monomer N-isopropylacrylamide (NIPAM) is used, microgels become thermoresponsive, with the network structure changing dramatically when the temperature exceeds the lower critical solution temperature (LCST) of approximately 33 °C (3–6). Below the LCST, microgels are soft and deformable, while above the LCST, the network expels water, leading to a denser polymer structure and repulsive or attractive hard sphere-like properties. Due to their tunability at biologically relevant temperatures and ease of synthesis, microgels have become popular in many areas of research. They act as drug carriers (7), viscosity modifiers (8), tunable colloidal depletants (9), scaffolds in tissue engineering (10, 11), and are useful for studying glass transition and jamming phenomena (12, 13). However, quantifying their mechanical properties remains challenging due to the combination of polymer physics and colloidal phenomena occurring.

At low concentrations, the colloidal nature of microgels dominates, and the suspension viscosity follows hard-sphere approximations such as the Einstein-Batchelor equation for the suspension's viscosity (14, 15). However, microgels are soft and flexible and can be overpacked "beyond" space-filling at higher concentrations, considering the volume fraction occupied by the unperturbed microgel size (16–18). As the concentration increases, the microgels come in contact and respond to the increased osmotic pressure exerted by their neighbors. Recent super-resolution microscopy studies revealed the different steps of the interaction (19). First, the microgels' corona compress, then they weakly interpenetrate, followed by deformation (faceting) of the core, and finally, isotropic compression. This results in a transition from the elastic behavior dominated by colloidal interactions towards properties of homogeneous polymer gels (20).

Previous rheological studies have identified the different interpenetration, deformation, and

isotropic compression stages (19, 21–24). The modulus G'_p shows a sharp increase during the onset of elasticity, associated with corona compression and interpenetration, followed by a linear increase for effective filling fractions above one where density fluctuations vanish. Several models have been proposed to describe the evolution of G'_p of microgel suspensions in a specific regime. Still, few have attempted to model the microgel’s elasticity over the entire range of concentrations (15, 22, 23, 25). Here, we present a framework that explicitly considers microgel jamming, deformation, and compression. Furthermore, our model spans the entire concentration range and globally has only one adjustable parameter.

Theory and Model

Our research aims to establish a link between the various stages of microgel interactions at different temperatures and the distinct elasticity regimes displayed by microgel suspensions and pastes. To achieve this, we consider submicron-sized poly-NIPAM microgels dispersed in water with an ionic strength of 5 mM KCl to screen residual charges carried by the ionic initiators, which is the most commonly studied microgel system. To quantitatively account for the different stages of packing, we propose a free energy minimization scheme. Specifically, we consider the increased number density and the vanishing free volume in stage I, the compression of the microgel corona in stage II, the faceting and compression of the core in stage III (as depicted in Fig. 1). We exclude the weak interdigitation observed in superresolution microscopy, which affects viscoelastic losses but is not expected to affect the elastic storage modulus substantially (19). Our modeling framework is derived from approach presented by Mason and Scheffold to model the elasticity of dense emulsions that display interfacial deformation (26). The model was later expanded to include the double layer repulsion in ionic emulsions by Kim et al. (27). Although we choose a similar approach, the interaction potential of microgels differs significantly from that of emulsion droplets (16, 19, 22). If Mason and co-workers’ model can be

extended to encompass microgels, it would introduce a relatively straightforward model capable of explaining the shear modulus in dense microgel suspensions. This would be a groundbreaking development, offering a simple tool applicable to various practical uses.

In our investigation, we aim to assess predictions for the elastic plateau modulus G'_p by comparing them to experimental results obtained from rheometry. We begin by examining

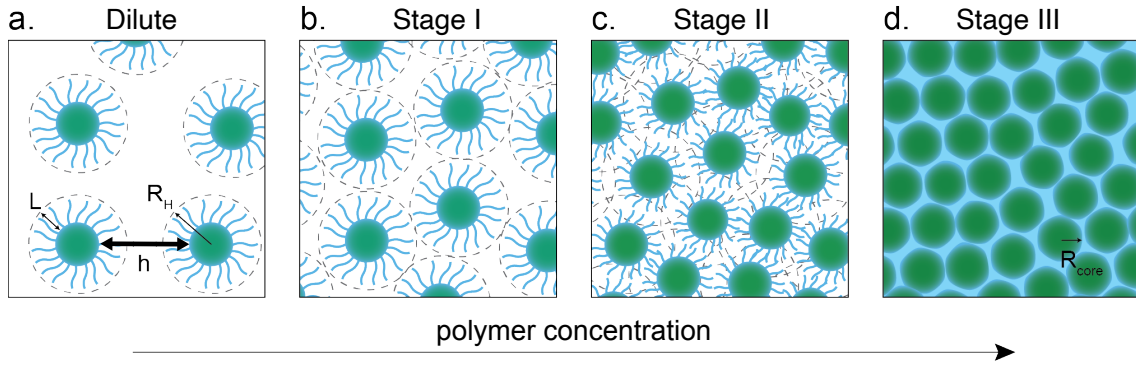


Figure 1: Sketch of microgel interactions and deformations with increasing concentration. **a** At low effective volume fractions the sample is in liquid state. Increasing volume fraction leads to a critical moment where coronae touch, shown in **b**. Dashed lines indicate the overall size of the microgel. **c** Further densification causes the corona to compress. **d** Once cores touch, they will deform. Length scales indicated are corona (brush) thickness L , The hydrodynamic radius $R_H \simeq R$, where R set the effective volume fraction ϕ . h denotes the separation distance between cores, and R_{core} the microgel core radius.

a dilute suspension of microgel particles, characterized by an effective volume fraction $\phi = \frac{N}{V} \frac{4}{3} \pi R^3$. $\frac{N}{V}$ denotes the number density, while R is the effective radius of the microgel particle, which is often assumed to be approximately equal to the hydrodynamic radius $R \simeq R_H$. As shown in Fig. 1 we also consider the core radius R_{core} and the corresponding core volume fraction $\zeta = \frac{N}{V} \frac{4}{3} \pi R_{\text{core}}^3$. Mason and Scheffold's model has defined the parameter $\zeta_d = \Delta V/V$ as the additional volume fraction that becomes available due to the deformation of the core caused by thermal fluctuations and shear strain (26) Considering a perturbative shear strain amplitude γ , the sample plateau shear modulus G'_p can be calculated.

We derive the plateau shear modulus by taking the derivative of the total free energy F_{tot} under the minimization condition $\zeta_d = \zeta_d^*$. We retain all parameters before evaluating the result at $\gamma \rightarrow 0$.

$$G'_p = \left| \frac{\delta F_{\text{tot}}}{\delta \gamma^2} \right|_{\zeta_d = \zeta_d^*, \gamma = 0} \quad (1)$$

Entropic contribution to the free energy

We consider amorphous suspensions; consequently, we expect to find a glass transition at an effective volume fraction of approximately $\phi \simeq 0.58$ (28, 29). As the system begins to solidify at the glass transition and beyond, entropic contributions to the free energy dominate due to (transient) particle caging by neighboring particles, leading to arrested motion and increased elasticity up to the critical volume fraction for random close packing (or jamming) of hard spheres where particles touch at approximately 0.646 volume fraction (30).

Table 1: Parameters for Modeling the Elastic Shear Modulus

Label	Meaning	Determined using
c	mass concentration (wt %)	drying, weighing
$k = \phi/c$	swelling ratio	Viscosity η ($\phi \ll 1$)
$\phi = \frac{N}{V} \frac{4}{3} \pi R^3$	effective volume fraction	$\phi = kc$
$R = \left(\frac{V}{N} \phi \right)^{\frac{1}{3}}$	effective radius (nm)	Number density $\frac{N}{V}$
$k_{\text{core}} = \zeta/c$	core swelling ratio	$\frac{G'_p}{\zeta(\zeta - 0.646)} = \frac{12}{10} \alpha (E^* \xi)$
$\zeta = \frac{N}{V} \frac{4}{3} \pi R_{\text{core}}^3$	core volume fraction	$\zeta = k_{\text{core}} c$
$R_{\text{core}} = \left(\frac{V}{N} \zeta \right)^{\frac{1}{3}}$	core radius (nm)	Number density $\frac{N}{V}$
L	corona thickness (nm)	$L = R - R_{\text{core}}$
E^*	core contact modulus (N/m ²)	$\frac{G'_p}{\zeta(\zeta - 0.646)} = \frac{12}{10} \alpha (E^* \xi)$
α, ξ	numerical constants, from (27)	$\alpha \simeq 1, \xi \simeq 0.15$
C	Brush elasticity (1/nm)	adjustable parameter

Contribution of the corona compression

Once the effective volume fraction surpasses a higher critical value of 0.646, the available free volume disappears, resulting in direct particle contacts and deformation (13, 30–32). The microgel corona, which have a lower crosslinker content than the microgel cores are compressed. This corona compression and its impact on elasticity have been extensively studied (19, 22–24, 33). One of the approaches to model corona repulsive interactions is based on the scaling model for a polymer brush, originally proposed by Alexander and de Gennes and later refined (34–36). It describes the repulsive force between two brush-coated surfaces, and it has been previously used to model the elasticity of the microgel corona in a good solvent (19, 22–24, 37). Here, we consider the mean field polymer theory treatment of the brush swelling and elasticity as summarized in reference (38). In this approximation, the polymer brush assumes a parabolic density profile. Using the Derjaguin approximation, the force between two particles coated with a polymer brush can be expressed as follows:

$$f(h) = -C(T) k_B T \frac{R_{\text{core}}}{L} \left[-\frac{1}{2u} - \frac{u^2}{2} + \frac{u^5}{10} + \frac{9}{10} \right] \quad (2)$$

where N_p is the degree of polymerization of the brush polymers, with $C(T) = 4\pi N_p^2 a^3 / s^4 \times \tau(T)$. By integration, we convert the force to energy per particle and obtain:

$$\frac{F_{\text{brush}}}{N k_B T} = C(T) \frac{R_{\text{core}}}{30} (u^6 - 10u^3 + 54u - 30 \log(u) - 45) \quad (3)$$

for $u = h/2L \leq 1$. The parameter h represents the distance between the surfaces of the microgel cores, while L stands for the equilibrium thickness of the polymer brush. The average distance between the polymer chains anchored on the microgel core is represented by s , and a is the typical size of a polymer molecule. Although water is a good solvent for pNIPAM microgels well below T_{LCST} , its quality deteriorates as T approaches T_{LCST} (38–40). This effect is captured by the dimensionless virial coefficient $\tau(T) = T_{\text{LCST}}/T - 1 \simeq 1 - T/T_{\text{LCST}}$ where

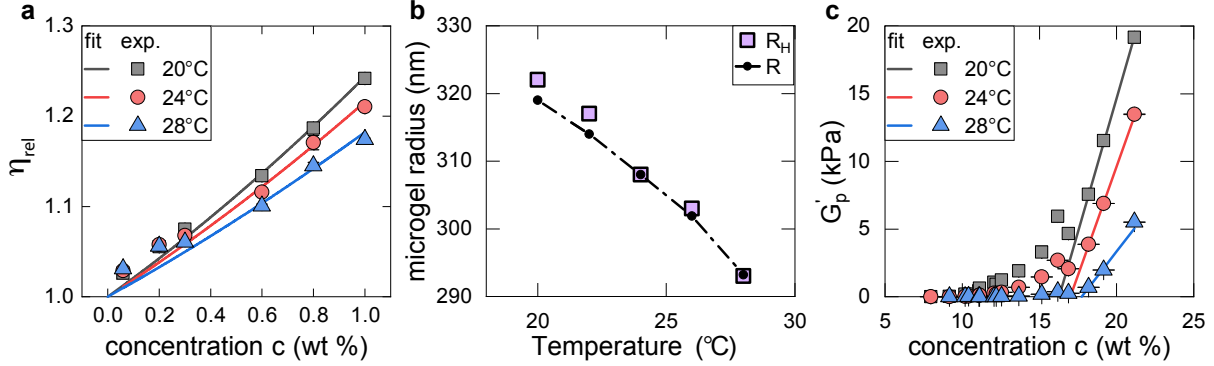


Figure 2: Experimental characterization of the system parameters. **a** Relative viscosity of low-concentration microgel samples (represented by symbols). Data shown was measured at temperatures 20, 24, and 28 °C with a rolling ball viscometer. The solid lines represent fits to the Einstein-Batchelor equation. **b** Full symbols and dashed line: Microgel (effective) particle radius (R) as a function of temperature obtained from the swelling ratio k and the number density N/V . Open squares indicate the hydrodynamic radius R_H measured through Dynamic Light Scattering (DLS). **c** Elastic modulus plateau values (G'_p) obtained through rheometry (represented by symbols), along with corresponding fits to the linear regime at the highest concentrations (solid lines).

$\tau(T) \propto A_2(T)$ is proportional to the experimentally accessible second virial coefficient. The linear decay of $A_2(T)$ was revealed experimentally for the single chain phase transition of pNIPAM by Kubota et al. (41), based on light scattering.

The relationship between h , the core volume fraction ζ , and the deformation volume fraction ζ_d was established by Kim et al. (27).

$$\frac{h}{R_{core}} \simeq 2 \cdot (0.646)^{1/3} [\zeta^{-1/3} - (0.646 + \zeta_d - \alpha\gamma^2)^{-1/3}] \quad (4)$$

where 0.646 is the jamming volume fraction of disordered spheres. In summary, we model corona interactions by employing a polymer brush model that considers the influence of solvent quality. Anticipated is a diminishing strength of brush repulsion as we approach the lower critical solution temperature (T_{LCST}).

Contribution of the microgel core deformation

When the particle concentration is high, the microgel corona becomes fully compressed onto the densely crosslinked core. Upon further increase of the microgel particle number density $\frac{N}{V}$, the microgel cores must undergo additional adaptation, as demonstrated in various studies (22, 23, 33, 40, 42–44). This adaptation results in deformation, faceting, and compression of the core, creating space for additional microgels. As observed in superresolution microscopy and neutron scattering studies, the microgel size decreases, indicating a volume change due to the softness of its core (16, 45). Seth, Cloitre, and Bonnecaze showed that the contact elastic modulus E^* of touching spheres can be related to the Laplace pressure in jammed emulsion droplets as $E^* \simeq 10\sigma/R$, where σ represents the surface tension of the droplets (46). The contact modulus E^* is further related to the Young's (bulk) modulus E and the Poisson's ratio ν through $E^* = E/[2(1 - \nu^2)]$ (46, 47). Using the results of ref. (26), we express the leading-order term in the free energy associated with particle core deformation as follows:

$$\frac{F_{\text{core}}}{N} = 4\pi \frac{E^*}{10} \xi R_{\text{core}}^3 \zeta_d^2 \quad (5)$$

where ξ is a dimensionless geometric parameter considering the entire disordered system. It encompasses the variously sized facets and different coordination numbers within the distribution of all particles.

Total free energy

The total free energy can now be written as:

$$F_{\text{tot}} = F_{\text{ent}} + F_{\text{brush}} + F_{\text{core}} \quad (6)$$

where F_{ent} denotes the entropic translational free energy $F_{\text{ent}} = -3Nk_{\text{B}}T \ln(0.646 + \zeta_d - \zeta - \alpha\gamma^2)$ (27). By inserting F_{tot} into (1), we analyze the shear modulus for different concentrations and various temperatures.

Shear modulus in the high concentration regime

It is helpful and informative to assess the plateau shear modulus under conditions where the corona term is omitted and $k_B T$ approaches zero. According to findings in (26), substituting σ/R by $E^*/10$ the corresponding formula for the shear modulus is:

$$G'_p(\zeta) = \frac{12}{10} \alpha E^* \xi \times \zeta (\zeta - 0.646) \quad (7)$$

This expression is expected to be the prevailing term for $\zeta > 0.646$. In the following, based on previous emulsion studies (26, 27), we set $\alpha = 1$ and $\xi = 0.15$ and consider E^* an effective core contact elasticity parameter.

Results and Discussion

Our model possesses a significant advantage in that we can independently determine all parameters through experiments, except for the corona elasticity parameter $C(T)$. To enhance clarity, we have included Table 1, which provides details on all model parameters along with information on how each is determined. In the following sections, we will elucidate our step-by-step approach. Additionally, it is worth noting that independent studies indicate that $C(T)$ is expected to linearly decay with temperature (41), reaching zero as it approaches T_{LCST} . Furthermore, it is anticipated that $E^*(T)$ will remain approximately constant, as suggested by previous research (48). We will leverage this information to validate our model assumptions. Initially, we determine the microgel concentration, denoted as c , in weight percent (wt %) by drying and weighing a specific amount of a diluted stock suspension. Subsequently, viscosity measurements are utilized to establish a relationship between c and the effective volume fraction ϕ of microgel samples, as referenced in previous works (15, 16, 24, 33, 49). When the effective volume fractions are low, the relative viscosity (denoted as $\eta_{rel} = \eta/\eta_h$) of microgel samples adheres to the Einstein-Batchelor equation with $\phi = kc$ (14, 50). In this scenario,

Table 2: Table of parameters utilized to characterize the experimental data presented in Fig. 3, acquired as outlined in the text.

Temperature (°C)	20	21	22	23	24	25	26	27	28
R (nm)	319.0	316.6	314.0	311.0	308.0	305.0	301.9	297.6	293.2
R_{core} (nm)	254.5	253.1	251.5	250.0	248.7	247.3	246.1	244.9	243.6
$L = R - R_{\text{core}}$ (nm)	64.5	63.5	62.5	61.0	59.3	57.7	55.9	52.7	49.6
k	0.08178	0.07989	0.07797	0.07579	0.07360	0.07145	0.06930	0.06640	0.06350
k_{core}	0.04150	0.04081	0.04004	0.03935	0.03874	0.03811	0.03752	0.03698	0.03641
E^* (N/m ²)	526183	534233	544965	544188	528307	502319	460258	397696	318656
C' (1/nm)	30.08	26.48	23.17	20.06	16.24	11.37	7.48	4.58	1.83

as per Brady and Vicic’s formulation, the expression for relative viscosity increase is given by $\eta_{\text{rel}} = \eta/\eta_h = 1 + 2.5kc + 5.9(kc)^2$, where η_h represents the viscosity of the surrounding medium, specifically water. By measuring a series of samples with a known concentration (c in wt %) and analyzing η_{rel} , we can determine the temperature-dependent shift factor, referred to as the swelling ratio k (see Fig. 2a). We determined the number density of particles N/V at a given c by imaging a known volume V using confocal microscopy and counting the particles therein. With knowledge of the number density, we can extract the effective radius R shown in Fig. 2b. The values obtained through this analysis compare well to the independently determined hydrodynamic radii obtained through dynamic light scattering, Fig. 2b. We use oscillatory shear measurements in a cone-plate configuration to determine the linear elastic shear modulus in the high-concentration regime, Figs. 2 and 3. In this context, we expect $G'_p(c) = \frac{12}{10}\alpha(E^*\xi) \times \zeta(c)(\zeta(c) - 0.646)$ with $\zeta(c) = c \cdot k_{\text{core}}$. By fitting the highest concentration data points, we obtain k_{core} and E^* . We have verified that the fit is stable to within a few percent by varying the number of points included in the analysis. With the knowledge of k_{core} and the number density N/V , we calculate the radius of the undeformed core R_{core} . We thus obtain the equilibrium thickness of the microgel corona via $L = R - R_{\text{core}}$.

The equilibrium thickness of the brush in the mean-field approximation is given by $L \sim N_p a (a/s)^{2/3} \tau(T)^{1/3}$, where, once again, $\tau(T) \simeq 1 - T/T_{\text{LCST}}$. In Fig. 4a, we compare the

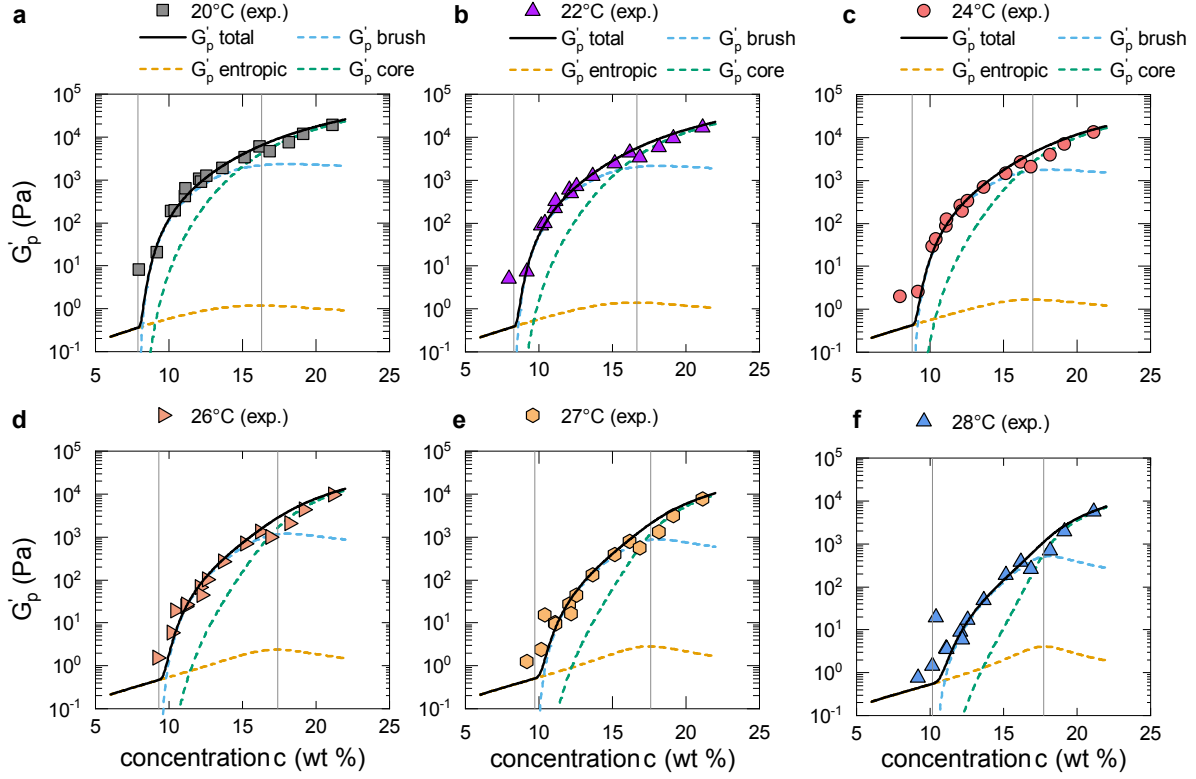


Figure 3: Global model fit to the experimental $G'_p(c, T)$ -data of the concentration-dependent shear modulus at various temperatures from **a** (20°) to **f** (28°). The elastic response's relative contribution from each of the three model terms is depicted individually as dashed colored lines.

experimental data with the theoretical prediction and observe excellent agreement for $T_{LCST} \sim 33^\circ\text{C}$ and $N_p a (a/s)^{2/3} \sim 190$ nm. With $a (a/s)^{2/3}$ on the order of 0.1 nm (for $a \sim 0.5$ nm and $s \sim 5$ nm), this suggests that the corona consists of chains with approximately $N_p \sim 1800$ monomer units. Here, we have chosen s to be comparable to the mesh size or correlation length of the cross-linked microgel core, on the order of a few nanometers ($5l$). The only remaining unknown parameter in the global model for $G'_p(c, T)$ is the parameter $C(T) = 4\pi N_p^2 a^3 / s^4 \times \tau(T)$, which determines the elasticity of the brush-like corona. For each temperature, we fit the model to the experimental data for $G'_p(c, T)$ across the entire concentration range by adjusting $C(T)$ and find excellent agreement as shown in Fig. 3. The values obtained for $C(T)$ at all

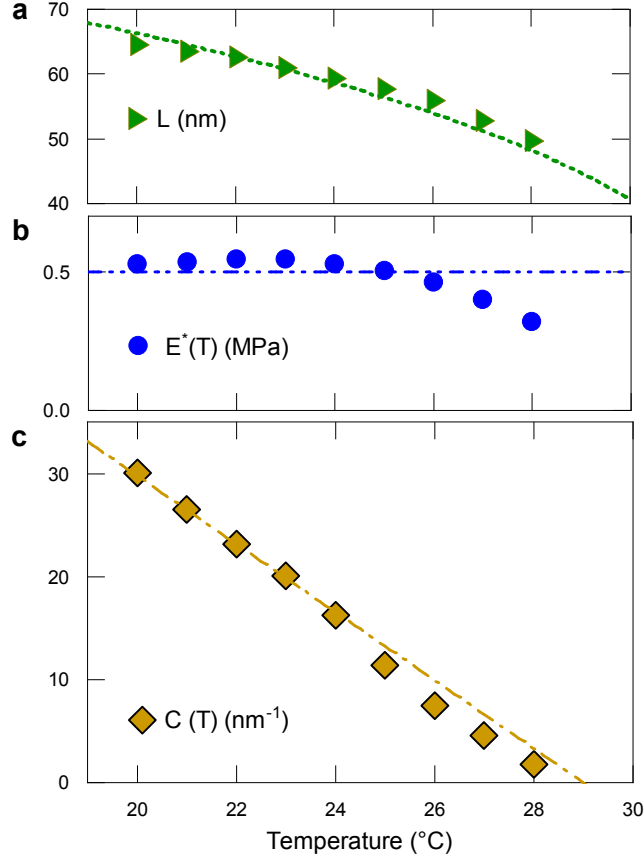


Figure 4: Temperature dependence of the model's parameters. **a** Equilibrium brush thickness $L = R - R_{\text{core}}$ (symbols). The dotted line shows the prediction by the mean-field model: $L = 190 \text{ nm} \times (1 - T/(306.15K))^{1/3}$ where the temperature T is expressed in Kelvin and the prefactor was adjusted for a best fit. **b** Contact elastic modulus E^* from a linear fit to $G'_p(c)$ in the high concentration regime. The line indicates a typical value of $E^* = 0.5\text{MPa}$. **c** Brush elasticity parameter in the mean-field-description, (3), obtained from a best global fit to the experimental data for $G'_p(c)$. The dash dotted line shows a linear fit to the data with $C(T) = 1000/\text{nm} \times (1 - T/(302.15K))$.

temperatures are listed in Table 2. Remarkably, we can even reproduce an unusual shoulder in the shear modulus for the highest temperatures, which, as now understood, arises from a decoupling of the brush elastic contribution to the core elastic contribution, Fig. 3f. The relative contribution of each of the three model terms to the elastic response is depicted individually as dashed colored lines.

In Fig. 4b and c, we present the temperature dependence of $E^*(T)$ and $C(T)$, respectively. As anticipated by polymer theory, the brush interactions soften as the solvent quality decreases when approaching the lower critical solution temperature (LCST) T_{LCST} (38). The parameter $C(T)$ decays linearly following $\tau(T) \simeq 1 - T/T_c$, where $T_c \sim 29^\circ\text{C}$ is found to be slightly smaller than $T_{\text{LCST}} \sim 33^\circ\text{C}$. The prefactor $C(T)/\tau(T) = 1000/\text{nm}$ is consistent with the same set of brush parameters discussed earlier: $N_p \sim 1800$, $a = 0.5\text{nm}$, and $s = 5\text{nm}$. With these numbers, $4\pi N_p^2 a^3/s^4 \simeq 500/\text{nm}$. Despite minor disagreements regarding the transition temperature in the fit, our model provides an excellent description of the shear elasticity of microgel suspensions and pastes from the low to high concentration regime, with good qualitative agreement with the molecular properties of the polymer microgels.

Summary and Conclusions

In summary, we present a free energy model describing the linear elastic shear modulus $G'_p(c, T)$ of concentrated microgel suspensions and pastes. In our approach, we minimize the free energy by considering particle interactions, accounting for the vanishing free volume entropic contribution, the compression of a soft polymer corona, and a homogeneous polymer gel core. The explicit treatment of the corona in the polymer brush framework is a cornerstone of our model. It enables us to quantify the onset of elasticity, and the brush parameters we find can be directly related to the microgel corona swelling curve $L(T)$, showcasing the consistency of the model. Notably, we find that the temperature dependence is well captured by the dimensionless virial coefficient, which quantifies the solvent quality for the microgel. A distinctive aspect of our approach is that we determine all parameters describing the system from oscillatory shear measurements, eliminating the need for indirect methods such as density profiles obtained from scattering or microscopy, which may not necessarily be representative for modeling the mechanical response. Our hierarchical model predicts constitutive properties of suspensions across

the entire range of concentrations and temperatures studied. It unravels the contributions from various mechanical modes, including the reduced free volume, the microgel corona, and the core, providing insights into particle behavior under external stress. This model possesses predictive power for calculating the elastic response under arbitrary conditions, particularly when the microgels are in a swollen state. Thus, it contributes to advancing our comprehension and utilization of polymer microgels in various fields.

Methods

Microgel synthesis

N-isopropylacrylamide (NIPAM, 97%, 7.20 g) and N,N'-Methylenebis(acrylamide) (BIS, 99%, 0.051524 g) were dissolved in 495 g of H₂O in a round-bottom flask. The solution was degassed with nitrogen at room temperature for 30 minutes. The temperature was then increased to 70°C, and the reaction mixture was allowed to reach equilibrium for 30 minutes. To initiate the reaction, potassium persulfate (KPS, 99%, 0.23273 g in 6.5 g H₂O) was injected. The reaction proceeded for 4 hours under a nitrogen atmosphere at 70°C. Afterward, the resulting solution was filtered using glass wool and subjected to dialysis for 2 weeks to remove any unreacted components. The mass concentration of the resulting solution was determined as 1.34 wt %, using drying and weighing. The mass density in wt % is defined as the ratio of the weight of the dried microgel component to the weight of the total sample.

Dynamic Light Scattering

We diluted a small amount of microgel stock solution (2 μ l) with 5 mM KCl in H₂O (200 μ l) and filled it into an NMR tube. The NMR tube was then placed inside a 3D-DLS light scattering spectrometer (LS Instruments, Switzerland), equipped with a laser that emitted light at a wavelength of 660 nm. The spectrometer collected scattered light within the range of angles from

40°C to 60°C, with a step size of 3°C. Measurements were conducted at various temperatures: 20°C, 24°C, 28°C, 30°C, 35°C, and 40°C. For each angle, three measurements were taken, each lasting 60 seconds. Before each measurement, the sample was allowed to reach thermal equilibrium at the target temperature for 30 minutes. The autocorrelation functions obtained from the measurements were subjected to standard second cumulant analysis to determine the hydrodynamic radius.

Viscometry

To conduct viscosity measurements, a pure solvent sample containing 5 mM KCl was prepared, along with several samples containing different concentrations of microgels (0.06 wt %, 0.1 wt %, 0.3 wt %, 0.6 wt %, and 1.0 wt %) in 5 mM KCl. The measurements were carried out at temperatures of 20°C, 22°C, 24°C, 26°C, and 28°C using a rolling ball viscometer (Anton Paar, Automated Microviscometer). Before each measurement, the samples were allowed to equilibrate at the respective temperature for 30 minutes. Ten repetitions of measurements a capillary with a diameter of 1.6 mm under an inclination angle of 40°, and using a ball with a diameter of 1.5 mm. To accurately determine the samples' viscosity, we also measured their mass densities at the same temperatures using a densimeter (Anton Paar, DSA 5000 M). After a 30-minute equilibration period, the density was measured twice. The relative viscosity, denoted as η_{rel} , was calculated by dividing the viscosity of each sample by the viscosity of the solvent.

Rheology

By centrifugation at 15,000 g for 30 minutes, we increased the mass density of the stock solution to 7 wt %. This elevated concentration yielded a dense liquid state at room temperature. Multiple rounds of centrifugation and controlled evaporation were performed at room temperature to obtain samples with higher concentrations. To adjust the salinity of the samples to 5

mM KCl, a specific amount of 1 M KCl electrolyte was added. Rheology measurements were conducted using a dilution series, where after each measurement, the remaining sample was diluted with 5 mM KCl and measured again. Rheology data was acquired using an Anton Paar rheometer (MCR300) in a cone-plate configuration. The cone had a radius of 25 mm, and the distance between the cone and the plate was 0.053 mm. A solvent trap was utilized during the measurements. Before the rheological measurement, the sample was heated to 30°C, and then 0.2 ml was transferred onto the pre-heated plate of the rheometer (maintained at 28°C) using a syringe. The sample was pre-sheared for 5 minutes at a shear rate of $\frac{d\gamma}{dt} = 100 \text{ s}^{-1}$. Subsequently, the temperature within the rheometer was gradually decreased from 30°C to 20°C at a rate of 0.5°C every 3 minutes. The values of G' and G'' were recorded at an amplitude of $\gamma = 0.1\%$ and an angular frequency of $\omega = 10 \text{ rad/s}$. Checks were carried out to ensure these measurements were conducted within the linear regime. Additionally, it was ensured that the sample reached equilibrium within 3 minutes, and a subsequent temperature cycle from 20°C back to 28°C was performed to confirm reproducibility.

References

1. L Andrew Lyon and Alberto Fernandez-Nieves. The polymer/colloid duality of microgel suspensions. *Annual Review of Physical Chemistry*, 63:25–43, 2012.
2. J Brijitta and P Schurtenberger. Responsive hydrogel colloids: Structure, interactions, phase behavior, and equilibrium and nonequilibrium transitions of microgel dispersions. *Current opinion in colloid & interface science*, 40:87–103, 2019.
3. Jianzhong Wu, Bo Zhou, and Zhibing Hu. Phase behavior of thermally responsive microgel colloids. *Physical Review Letters*, 90(4):048304, 2003.

4. Markus Stieger, Walter Richtering, Jan Skov Pedersen, and Peter Lindner. Small-angle neutron scattering study of structural changes in temperature sensitive microgel colloids. *The Journal of Chemical Physics*, 120(13):6197–6206, 2004.
5. TG Mason and MY Lin. Density profiles of temperature-sensitive microgel particles. *Physical Review E*, 71(4):040801, 2005.
6. Mathias Reufer, Pedro Diaz-Leyva, Iseult Lynch, and Frank Scheffold. Temperature-sensitive poly (n-isopropyl-acrylamide) microgel particles: A light scattering study. *The European Physical Journal E*, 28(2):165–171, 2009.
7. Jung Kwon Oh, Ray Drumright, Daniel J Siegwart, and Krzysztof Matyjaszewski. The development of microgels/nanogels for drug delivery applications. *Progress in polymer science*, 33(4):448–477, 2008.
8. Efren Andablo-Reyes, Demetra Yerani, Ming Fu, Evangelos Lias, Simon Connell, Ophelie Torres, and Anwesha Sarkar. Microgels as viscosity modifiers influence lubrication performance of continuum. *Soft Matter*, 15(47):9614–9624, 2019.
9. Stefano Sacanna, William TM Irvine, Paul M Chaikin, and David J Pine. Lock and key colloids. *Nature*, 464(7288):575–578, 2010.
10. Tiantian Gan, Ying Guan, and Yongjun Zhang. Thermogelable pnipam microgel dispersion as 3d cell scaffold: effect of syneresis. *Journal of Materials Chemistry*, 20(28):5937–5944, 2010.
11. Tapomoy Bhattacharjee, Carmen J Gil, Samantha L Marshall, Juan M Uruenña, Christopher S O’Bryan, Matt Carstens, Benjamin Keselowsky, Glyn D Palmer, Steve Ghivizzani, C Parker Gibbs, et al. Liquid-like solids support cells in 3d. *ACS Biomaterials Science & Engineering*, 2(10):1787–1795, 2016.

12. Zexin Zhang, Ning Xu, Daniel TN Chen, Peter Yunker, Ahmed M Alsayed, Kevin B Aptowicz, Piotr Habdas, Andrea J Liu, Sidney R Nagel, and Arjun G Yodh. Thermal vestige of the zero-temperature jamming transition. *Nature*, 459(7244):230–233, 2009.
13. Atsushi Ikeda, Ludovic Berthier, and Peter Sollich. Disentangling glass and jamming physics in the rheology of soft materials. *Soft Matter*, 9(32):7669–7683, 2013.
14. GK Batchelor. The effect of brownian motion on the bulk stress in a suspension of spherical particles. *Journal of fluid mechanics*, 83(1):97–117, 1977.
15. H Senff and W Richtering. Temperature sensitive microgel suspensions: Colloidal phase behavior and rheology of soft spheres. *The Journal of Chemical Physics*, 111(4):1705–1711, 1999.
16. Gaurasundar M Conley, Philippe Aebischer, Sofi Nöjd, Peter Schurtenberger, and Frank Scheffold. Jamming and overpacking fuzzy microgels: Deformation, interpenetration, and compression. *Sci. Adv.*, 3(10):e1700969, 2017.
17. Izabella Bouhid de Aguiar, Ties Van de Laar, Martine Meireles, Antoine Bouchoux, Joris Sprakel, and Karin Schroën. Deswelling and deformation of microgels in concentrated packings. *Scientific Reports*, 7(1):1–11, 2017.
18. Svetoslav V Nikolov, Alberto Fernandez-Nieves, and Alexander Alexeev. Behavior and mechanics of dense microgel suspensions. *Proceedings of the National Academy of Sciences*, 117(44):27096–27103, 2020.
19. Gaurasundar M Conley, Chi Zhang, Philippe Aebischer, James L Harden, and Frank Scheffold. Relationship between rheology and structure of interpenetrating, deforming and compressing microgels. *Nat. Comm.*, 10(1):1–8, 2019.

20. Paul Menut, Sebastian Seiffert, Joris Sprakel, and David A Weitz. Does size matter? elasticity of compressed suspensions of colloidal-and granular-scale microgels. *Soft matter*, 8(1):156–164, 2012.
21. Michel Cloitre, Régis Borrega, Fabrice Monti, and Ludwik Leibler. Structure and flow of polyelectrolyte microgels: from suspensions to glasses. *Comptes Rendus Physique*, 4(2):221–230, 2003.
22. Frank Scheffold, Pedro Díaz-Leyva, Mathias Reufer, Nasser Ben Braham, Iseult Lynch, and James L Harden. Brushlike interactions between thermoresponsive microgel particles. *Physical Review Letters*, 104(12):128304, 2010.
23. Giovanni Romeo and Massimo Pica Ciamarra. Elasticity of compressed microgel suspensions. *Soft Matter*, 9(22):5401–5406, 2013.
24. Andrea Scotti, Monia Brugnoli, Carlos G Lopez, Steffen Bochenek, Jérôme J Crassous, and Walter Richtering. Flow properties reveal the particle-to-polymer transition of ultra-low crosslinked microgels. *Soft Matter*, 16(3):668–678, 2020.
25. Ashesh Ghosh, Gaurav Chaudhary, Jin Gu Kang, Paul V Braun, Randy H Ewoldt, and Kenneth S Schweizer. Linear and nonlinear rheology and structural relaxation in dense glassy and jammed soft repulsive pnipam microgel suspensions. *Soft Matter*, 15(5):1038–1052, 2019.
26. Thomas G Mason and Frank Scheffold. Crossover between entropic and interfacial elasticity and osmotic pressure in uniform disordered emulsions. *Soft Matter*, 10(36):7109–7116, 2014.

27. Ha Seong Kim, Frank Scheffold, and Thomas G Mason. Entropic, electrostatic, and interfacial regimes in concentrated disordered ionic emulsions. *Rheol. Acta*, 55(8):683–697, 2016.
28. Ulf Bengtzelius, W Gotze, and A Sjolander. Dynamics of supercooled liquids and the glass transition. *Journal of Physics C: Solid State Physics*, 17(33):5915, 1984.
29. Peter N Pusey and William van Megen. Observation of a glass transition in suspensions of spherical colloidal particles. *Physical Review Letters*, 59(18):2083, 1987.
30. Salvatore Torquato, Thomas M Truskett, and Pablo G Debenedetti. Is random close packing of spheres well defined? *Physical Review Letters*, 84(10):2064, 2000.
31. JD Bernal and J Mason. Packing of spheres: co-ordination of randomly packed spheres. *Nature*, 188(4754):910–911, 1960.
32. Atsushi Ikeda, Ludovic Berthier, and Peter Sollich. Unified study of glass and jamming rheology in soft particle systems. *Physical Review Letters*, 109(1):018301, 2012.
33. Maxime J Bergman, Nicoletta Gnan, Marc Obiols-Rabasa, Janne-Mieke Meijer, Lorenzo Rovigatti, Emanuela Zaccarelli, and Peter Schurtenberger. A new look at effective interactions between microgel particles. *Nature Communications*, 9(1):1–11, 2018.
34. S Alexander. Adsorption of chain molecules with a polar head a scaling description. *Journal De Physique*, 38(8):983–987, 1977.
35. PrG de Gennes. Conformations of polymers attached to an interface. *Macromolecules*, 13(5):1069–1075, 1980.

36. Ekaterina B Zhulina, Oleg V Borisov, and Victor A Priamitsyn. Theory of steric stabilization of colloid dispersions by grafted polymers. *Journal of colloid and interface science*, 137(2):495–511, 1990.
37. Huilin Tu, Liang Hong, Stephen M Anthony, Paul V Braun, and Steve Granick. Brush-sheathed particles diffusing at brush-coated surfaces in the thermally responsive pnipaaam system. *Langmuir*, 23(5):2322–2325, 2007.
38. Rosa M Espinosa-Marzal, Prathima C Nalam, Sreenath Bolisetty, and Nicholas D Spencer. Impact of solvation on equilibrium conformation of polymer brushes in solvent mixtures. *Soft Matter*, 9(15):4045–4057, 2013.
39. Fabrizio Camerin, Nicoletta Gnan, Lorenzo Rovigatti, and Emanuela Zaccarelli. Modelling realistic microgels in an explicit solvent. *Scientific Reports*, 8(1):1–12, 2018.
40. Letizia Tavagnacco, Ester Chiessi, and Emanuela Zaccarelli. Molecular insights on poly (n-isopropylacrylamide) coil-to-globule transition induced by pressure. *Physical Chemistry Chemical Physics*, 23(10):5984–5991, 2021.
41. Kenji Kubota, Shouei Fujishige, and Isao Ando. Single-chain transition of poly (n-isopropylacrylamide) in water. *Journal of Physical Chemistry*, 94(12):5154–5158, 1990.
42. Nicoletta Gnan, Lorenzo Rovigatti, Maxime Bergman, and Emanuela Zaccarelli. In silico synthesis of microgel particles. *Macromolecules*, 50(21):8777–8786, 2017.
43. Lorenzo Rovigatti, Nicoletta Gnan, and Emanuela Zaccarelli. Internal structure and swelling behaviour of in silico microgel particles. *Journal of Physics: Condensed Matter*, 30(4):044001, 2017.

44. Lorenzo Rovigatti, Nicoletta Gnan, Andrea Ninarello, and Emanuela Zaccarelli. Connecting elasticity and effective interactions of neutral microgels: The validity of the hertzian model. *Macromolecules*, 52(13):4895–4906, 2019.
45. U Gasser, JS Hyatt, J-J Lietor-Santos, ES Herman, L Andrew Lyon, and A Fernandez-Nieves. Form factor of pnipam microgels in overpacked states. *The Journal of chemical physics*, 141(3), 2014.
46. Jyoti R Seth, Michel Cloitre, and Roger T Bonnecaze. Elastic properties of soft particle pastes. *Journal of Rheology*, 50(3):353–376, 2006.
47. Judith Elizabeth Houston, Lisa Fruhner, Alexis de la Cotte, Javier Rojo González, Alexander Valerievich Petrunin, Urs Gasser, Ralf Schweins, Jürgen Allgaier, Walter Richtering, Alberto Fernandez-Nieves, et al. Resolving the different bulk moduli within individual soft nanogels using small-angle neutron scattering. *Science Advances*, 8(26):eabn6129, 2022.
48. Panayiotis Voudouris, Daniel Florea, Paul van der Schoot, and Hans M Wyss. Micromechanics of temperature sensitive microgels: dip in the poisson ratio near the lcst. *Soft Matter*, 9(29):7158–7166, 2013.
49. Priti S Mohanty, Sofi Nöjd, Kitty van Gruijthuijsen, Jérôme J Crassous, Marc Obiols-Rabasa, Ralf Schweins, Anna Stradner, and Peter Schurtenberger. Interpenetration of polymeric microgels at ultrahigh densities. *Scientific Reports*, 7(1):1487, 2017.
50. John F Brady and Michael Vicic. Normal stresses in colloidal dispersions. *Journal of Rheology*, 39(3):545–566, 1995.
51. JJ Lietor-Santos, U Gasser, R Vavrin, ZB Hu, and A Fernandez-Nieves. Structural changes of poly (n-isopropylacrylamide)-based microgels induced by hydrostatic pressure and tem-

perature studied by small angle neutron scattering. *The Journal of chemical physics*, 133(3), 2010.

Data availability

All experimental data and model output discussed in the manuscript will be uploaded to the repository Zenodo (xxxxxxx). All additional data sets generated during and/or analyzed during the current study are available from the corresponding author upon reasonable request.

Competing interest

The authors declare no competing interest.

Author Contributions

MJB, TGM and FS designed the study. MJB performed most of the experiments and performed the initial data analysis. CZ contributed to the data analysis and carried out some additional experiments. FS and TGM derived the theoretical model. YX coded the model under the supervision of TGM. FS and MJB drafted the manuscript with contributions from all authors. All authors contributed to analyzing, interpreting, and revising the final version of the manuscript.

Acknowledgments

The Swiss National Science Foundation funded this project through the National Center of Competence in Research Bio-Inspired Materials, project No. 205603, and through project No. 188494. This work was supported by the University of California, Los Angeles. M.J.B. is grateful to Francois Lavergne for his assistance with rheology measurements.